Physics in Medicine & Biology

IPEM Institute of Physics and Engineering in Medicine

PAPER

Individualized adjustments to reference phantom internal organ dosimetry—scaling factors given knowledge of patient internal anatomy

To cite this article: Michael B Wayson and Wesley E Bolch 2018 *Phys. Med. Biol.* **63** 085006

INDIVIDUALIZED ADJUSTMENTS TO REFERENCE PHANTOM INTERNAL ORGAN DOSIMETRY – SCALING FACTORS GIVEN KNOWLEDGE OF PATIENT INTERNAL ANATOMY

Michael B. Wayson and Wesley E. Bolch
J. Crayton Pruitt Family Dept. of Biomedical Engineering, University of Florida, Gainesville, FL

PRESENT ADDRESS:
Michael B Wayson, PhD, DABR, DABSNM
Medical Physics and Radiation Safety
Baylor Scott & White Health
3500 Gaston Avenue
Dallas , TX 75246

FOR REPRINTS AND CORRESPONDENCE CONTACT:
Wesley E. Bolch, PhD, PE, CHP
J. Crayton Pruitt Family Department of Biomedical Engineering
University of Florida, Gainesville, Florida 32611-8300
Phone: (352) 273-0303 Fax: (352) 294-7126 Email: wbolch@ufl.edu

SHORT TITLE:
S Value Adjustments by Patient Organ Size and Position

This work was supported by:
NCI Grant R01 CA116743
NCI Grant R01 CA096441
US DOE Grant DE-FG07-06ID14773

Counts:
Abstract – 287 words
Manuscript – 8203 words (including table and figure captions)
Tables – 8
Figures – 11

SUMBITTED TO: *Physics in Medicine and Biology*

ABSTRACT

Various computational tools are currently available that facilitate patient organ dosimetry in diagnostic nuclear medicine, yet they are typically restricted to reporting organ doses to ICRP-defined reference phantoms. The present study, while remaining computational phantom based, provides straightforward tools to adjust reference phantom organ dose for both internal photon and electron sources. A wide variety of monoenergetic specific absorbed fractions (SAFs) were computed using radiation transport simulations for tissue spheres of varying size and separation distance. Scaling methods were then constructed for both photon and electron self-dose and cross-dose, with data validation provided from patient-specific voxel phantom simulations, as well via comparison to the scaling methodology given in MIRD Pamphlet No. 11. Photon and electron self-dose was found to be dependent on both radiation energy and sphere size. Photon cross-dose was found to be mostly independent of sphere size. Electron cross-dose was found to be dependent on sphere size when the spheres were in close proximity, owing to differences in electron range. The validation studies showed that this dataset was more effective than the MIRD 11 method at predicting patient-specific photon doses for at both high and low energies, but gave similar results at photon energies between 100 keV and 1 MeV. The MIRD 11 method for electron self-dose scaling was accurate for lower energies but began to break down at higher energies. The photon cross-dose scaling methodology developed in this study showed gains in accuracy of up to 9% for actual patient studies, and the electron cross-dose scaling methodology showed gains in accuracy up to 9% as well when only the bremsstrahlung component of the cross-dose was scaled. These dose scaling methods are readily available for incorporation into internal dosimetry software for diagnostic phantom-based organ dosimetry.

Keywords: Nuclear medicine dosimetry, patient-specific dose scaling, specific absorbed fraction, dose sensitivity.

1. Introduction

When patients undergo nuclear medicine imaging or therapy procedures, the radiation absorbed dose to various internal organs is of high clinical interest. Estimates of internal organ dose are needed to optimize the administered activity in radiopharmaceutical therapy thereby maximizing tumor cell kill while minimizing normal tissue toxicity (e.g., bone marrow, kidneys, lungs, and small intestinal walls). In diagnostic imaging, dose optimization takes the form of maximizing image quality while minimizing stochastic cancer risk, where the dose estimate to known radiosensitive organs is a requirement. More accurate internal dose estimates would allow for individual site-specific risk estimates. These could be used to more effectively optimize imaging protocols as the radiological protection quantity *effective dose* only applies to a population average. In both areas of nuclear medicine, accurate and patient-specific estimates of organ dose are sought which are clinically feasible to obtain.

In radionuclide therapy, the ideal computational model of the patient's internal anatomy, as needed to assess both organ self-dose and organ cross-dose, would derive from a CT (or potentially as MR) image of the individual patient in manner analogous to the clinical workflow in external beam radiotherapy. In diagnostic nuclear medicine, however, dose estimates have been based historically on stylized anatomic patient models (Cristy and Eckerman, 1987) and the MIRD internal dosimetry schema (Bolch *et al.*, 2009). Voxel phantoms, and most recently, hybrid computational phantoms – based upon NURBS and/or polygon mesh surfaces – are improvements over stylized models as they more closely represent true internal anatomy (Xu and Eckerman, 2009; Bolch *et al.*, 2010). Hybrid computational phantoms still predominately represent reference individuals of the International Commission on Radiological Protection (ICRP) and are frequently used for internal dosimetry (Lee *et al.*, 2010; Stabin *et al.*, 2012; Zhang *et al.*, 2009; Xu *et al.*, 2007; Yeom *et al.*, 2016a; Yeom *et al.*, 2016b; Kim *et al.*, 2017). Reference phantoms apply to the average individual by height and weight at fixed intervals of age (ICRP, 2002). These phantoms may be applied for estimates of internal organ

dose for individual patients, but there is a high probability that the patient for whom the dosimetry is being performed would not be 50th percentile in neither height nor weight. In such cases, dose estimates based on the hybrid reference phantoms are more desirable than estimates using simplified models, but they are still not likely to represent the internal anatomy of nuclear medicine patient.

In the current study, dosimetric sensitivity studies were performed to characterize changes in radiation absorbed dose with changes in a variety of measureable parameters. The goal was to develop equations that could be implemented within an internal dosimetry software package or to generate sets of look-up-table (LUT)-style scaling factors. These equations, or scaling factors, would require input from either knowledge of the patient's internal anatomy (e.g., organ masses and inter-organ separation distances) or external anatomy (e.g., patient weight and sitting height). Based on these inputs, the reference specific absorbed fractions (SAFs) could be scaled to better predict actual organ doses in the patient of interest.

SAF represents the fraction of energy emitted by a source organ where a radiopharmaceutical accumulates that is absorbed per unit mass by a target organ and is given by Equation 1 as described in both MIRD Pamphlet No. 21 (Bolch *et al.*, 2009) and ICRP Publication 130 (ICRP, 2015):

$$\Phi(r_T \leftarrow r_S, E_o) = \frac{\phi(r_T \leftarrow r_S, E_o)}{m_T} \quad (1)$$

where $\phi(r_T \leftarrow r_S, E_o)$ is the absorbed fraction (AF) of energy (fraction of energy deposited in the target tissue that was emitted by the source tissue) for target tissue r_T, source tissue r_S, and radiation energy E_o.

SAFs are used to calculate radionuclide-specific S values, which are the radiation absorbed dose in the target organ per unit nuclear transformation in the source organ. The S value is described in Equation 2:

$$S(r_T \leftarrow r_S) = \sum_i E_i Y_i \Phi(r_T \leftarrow r_S, E_i) \quad (2)$$

where $S(r_T \leftarrow r_S)$ is the radionuclide S value from source tissue r_S to target tissue r_T, E_i is the initial energy of the i^{th} radiation in the spectrum, Y_i is the yield of the i^{th} radiation in the spectrum, and $\Phi(r_T \leftarrow r_S, E_i)$ is the SAF for source tissue r_S irradiating target tissue r_T for radiation energy E_i.

Dose scaling in this study is proposed to be applied to SAFs rather than S values because it was hypothesized that SAFs scale differently for different initial radiation energies, source/target combinations, and organ sizes. Thus, the methods proposed here would provide patient-specific adjustments to the monoenergetic photon and electron SAFs, after which the radionuclide S values would be re-computed. If each component SAF of the S value scales differently, a single scaling factor cannot be applied to the S value.

Other studies have examined dosimetric sensitivity to varying degrees (Stabin and Konijnenberg, 2000; Clark *et al.*, 2010; Marine *et al.*, 2010). These studies have demonstrated the importance of considering differences in patient body habitus and changes in source organ and target organ sizes. Organ self-dose, where the source and target organ are the same, has been previously addressed by MIRD Pamphlet No. 11 (Snyder *et al.*, 1975). It was recommended in that report that self-dose SAFs should be scaled for non-reference organ sizes by the inverse ratio of the organ masses to a constant power. The value of the power was set to $-2/3$ for photon self-dose scaling and –1 for electron self-dose scaling. The current study attempts to improve the MIRD self-dose model to include dependence on initial radiation energy, reference source organ mass, and non-reference target organ mass. The largest absorbed doses resulting from a given source organ are observed when the source and target are the same organ, and thus dose scaling techniques for self-irradiation are important.

The overall objective of the current study is thus to adjust internal dosimetry estimates from the University of Florida (UF) reference phantoms (Lee *et al.*, 2010)[1] to individual patients with prior knowledge of patient organ size and/or inter-organ separation. The study individually explores photon and electron scaling factors for both organ self-dose and organ cross-dose. For organ self-dose, the developed scaling factors are compared to the energy-independent recommendations from MIRD Pamphlet No. 11. In a related study, we explore similar techniques based upon only knowledge of the patient's external body morphometry (Wayson and Bolch, in review).

2. Materials and Methods

The present study utilizes a variety of computational models for differing computed quantities and for different modeling purposes as summarized in Table 1 below. This table may be used as a reference for the discussions to follow.

Table 1. Overview of computational models used in the current study.

Computational Model	Purpose	Computed Quantity
Spheres of different sizes	Sensitivity study (self-dose)	SAF scaling factors
Spheres of different sizes and center-to-center separations	Sensitivity study (cross-dose)	Matrix of SAF values for interpolation
UF hybrid phantoms	Validation study (self- and cross-dose)	Estimated S value calculated using scaled reference SAFs
Patient-specific phantom based on actual CT images	Validation study (self- and cross-dose)	Actual or "gold standard" S value

[1] Phantom nomenclature for the UF hybrid reference series includes: UFH00MF (newborn male and female), UF01MF (1-year-old male and female), UF05MF (5-year-old male and female), UF10MF (10-year-old male and female), UF15M (15-year-old male), UF15F (15-year-old female), UFHADM (adult male), UFHADF (adult female).

2.1 Photon and Electron Self-Dose

2.1.1 Self-Dose Simulations A computational study using the MCNPX v2.6 radiation transport code was designed to examine the relationship between radiation absorbed dose and source/target region size when the source and target region are the same (self-dose). Twenty-one spheres were constructed with masses ranging from $1\,g$ to $10\,kg$. The spheres were assigned a density of $1.0\ g/cm^3$ and a tissue composition of average adult male soft tissue, as defined in Report 46 of the International Commission on Radiation Units and Measurements (ICRU) (ICRU, 1992). The surrounding medium consisted of this same tissue and represented an "infinite" surrounding medium. Monoenergetic photons and electrons of 21 energies between 10 keV and 4 MeV were individually simulated. Uniform photon and electron sources were simulated within each source sphere, and the energy deposited in the source sphere was recorded. Based on MIRD Pamphlet No. 11 (Snyder *et al.*, 1975), the non-reference self-dose SAF can be calculated according to Equation 3, and the scaling power R is then given as Equation 4. SAFs for all simulated combinations of tissue masses and radiation energies were computed, and the resulting value of $R\left(E_o, m_{ref}, m_{non-ref}\right)$ was determined using Equation 4:

$$\Phi\left(r \leftarrow r, E_o, m_{non-ref}\right) = \Phi\left(r \leftarrow r, E_o, m_{ref}\right)\left(\frac{m_{non-ref}}{m_{ref}}\right)^{R\left(E_o, m_{ref}, m_{non-ref}\right)} \quad (3)$$

$$R\left(E_o, m_{ref}, m_{non-ref}\right) = \frac{log\left[\frac{\Phi\left(r \leftarrow r, E_o, m_{non-ref}\right)}{\Phi\left(r \leftarrow r, E_o, m_{ref}\right)}\right]}{log\left(\frac{m_{non-ref}}{m_{ref}}\right)} \quad (4)$$

where $\Phi\left(r \leftarrow r, E_o, m_{non-ref}\right)$ is the self-dose SAF for tissue r at initial radiation energy E_o for non-reference tissue mass $m_{non-ref}$, $\Phi\left(r \leftarrow r, E_o, m_{ref}\right)$ is the self-dose SAF for tissue r at initial radiation energy E_o for the reference tissue mass m_{ref}, and $R\left(E_o, m_{ref}, m_{non-ref}\right)$ is the scaling power as a

function of initial radiation energy E_o, reference tissue mass m_{ref}, and non-reference tissue mass $m_{non-ref}$.

Equation 3 was used to derive the self-dose mass ratio scaling powers, R. At each photon energy, the SAF of each original sphere mass (termed the "reference" sphere mass) was divided by the SAFs of all other sphere masses (termed the "non-reference" sphere masses). The masses of each sphere were already defined, and so R was computed using Equation 4 for each energy/reference mass/non-reference mass combination.

2.1.2 Self-Dose Validation Studies For all validation studies in this manuscript, the process involved a patient-specific phantom developed from actual patient CT scans and the relevant reference phantom from the UF hybrid phantom library. S values were calculated from simulation of sources in the patient-specific phantom. S values were also calculated by scaling SAFs for the relevant UF hybrid reference phantom using scaling techniques developed in the current study. These two S values were compared, and the relative merit of dose scaling was assessed.

Patient-specific voxel phantoms constructed by Johnson *et al* (2011) were used to validate the derived self-dose scaling powers. These patient-specific phantoms were generated by segmenting CT image sets of each patient to create three-dimensional organ and body volumes. CT image sets of 14 adult male patients and 13 adult female patients covering broad ranges of height and weight were segmented to create the patient-specific phantoms (Johnson *et al.*, 2011). Tissues in the head and legs were not present because the CT image sets were chest-abdomen-pelvis (CAP) scans. Several organs were difficult to visualize in the scans, so only the pericardium, liver, lungs, spleen, stomach wall, stomach contents, pancreas, kidneys, urinary bladder wall, urinary bladder contents, skeleton, subcutaneous fat, and outer body contour were segmented. All phantoms were voxelized at an isotropic resolution of 2 mm.

BEXXAR® (^{131}I −Tositumomab) and Zevalin® (^{90}Y −ibritumomab tiuxetan) were selected as the radiopharmaceuticals for which radionuclide S values would be calculated with ^{131}I and ^{90}Y as the radionuclides of interest. ICRP Publication 107 was consulted for radionuclide spectra for ^{131}I and ^{90}Y (ICRP, 2008). Photons were simulated for ^{131}I, and beta particles were simulated for ^{90}Y. The package inserts for BEXXAR® and Zevalin® were consulted (as well as a case study for BEXXAR®)[2] to determine possible source tissues for simulation. The liver and spleen were selected as the source tissues, and all tissues segmented in the patient-specific phantoms were treated as target tissues. Liver and spleen self-dose were of interest for the self-dose validation studies.

Radionuclide spectra were directly sampled and uniformly distributed throughout each source tissue. Energy deposition in all target tissues was recorded, and the radionuclide S value was calculated using Equation 2. Tissue densities and material compositions were taken from ICRP Publication 89 (ICRP, 2002). Ten million particle histories were simulated to ensure adequately low uncertainties.

The relevant UF reference phantom liver and spleen self-dose SAFs (reported in Wayson *et al* (2012)) were scaled using the calculated mass ratio scaling factors based on the derived scaling power *R* as a function of radiation energy and source/target tissue size. These scaled SAFs were used to calculate the scaled S values. Finally, the scaled S values were then compared to the liver and spleen self-dose S values obtained from the CT image-based patient-specific MCNPX v2.6 simulations discussed above.

2.2 Photon and Electron Cross-Dose

2.2.1 Cross-Dose Simulations A computational study using MCNPX v2.6 was designed to examine the relationship between radiation absorbed dose and source/target region size and separation when the source and target region are different (cross-dose). Seventeen spheres were constructed with

[2] http://gamma.wustl.edu/newtfh/general/combined/small_118421.html

masses of 1 g to 2 kg since 2 kg was the upper limit for discrete (non-distributed) organ masses in the UF adult male hybrid computational phantom (Lee *et al.*, 2010). The spheres were assigned a density of 1.0 g/cm^3 and a tissue composition of average adult male soft tissue, as defined by ICRU Report 46 (ICRU, 1992). The surrounding medium consisted of ICRU Report 46 average adult male soft tissue and represented an "infinite" surrounding medium.

Each sphere mass was simulated as a source tissue, with every sphere included as a target tissue. The set of target spheres was incrementally placed away from the source sphere with an initial center-to-center separation of 16 cm, approximately equal to the diameter of the largest sphere, and a final center-to-center separation of 100 cm, greater than the largest discrete organ-to-organ separation seen in the UF hybrid phantom family ($\sim$75 cm from the urinary bladder wall to the brain in the UF adult male phantom) with a total of five equal increments.

To further explore the possibility of cross-dose scaling at medium-to-close distance separations, a similar cross-dose computational experiment was designed allowing for center-to-center separations less than 15.63 cm. Separations of 3.37 cm, 6.74 cm, 10.10 cm, and 13.47 cm and sphere masses of 1 g, 2 g, 4 g, 6 g, 8 g, 10 g, and 20 g were used. The number of sphere masses was limited due to overlap when larger spheres were located at these center-to-center distances (e.g., the 2 kg sphere radius of 7.82 cm would cause the spheres to overlap when their center-to-center distance was 3.37 cm).

Monoenergetic photons and electrons of 21 energies between 10 keV and 4 MeV were individually simulated. Particle histories between 10^8 (for 10 keV)[3] and 10^7 (for 4 MeV) were simulated to ensure adequately low uncertainties. Energy deposition accounting for all photons and electrons created during the simulation was recorded in all target spheres. The SAFs for all source-

[3] Ten million particle histories were simulated for all energies in the self-dose study because uncertainties are much lower in the self-dose irradiation geometry. Uncertainties increase as source-target separation increases since it is less likely the target will experience an interaction with any given emitted radiation.

target-energy combinations were calculated as the energy deposited in the target tissue of interest divided by the mass of the target tissue and the initial energy of the radiation.

Reverse Monte Carlo was performed for all sphere combinations, and the SAF of the source-target combination with the lowest statistical uncertainty was retained. Reverse Monte Carlo takes advantage of the reciprocity theorem that states that the SAF for a source tissue irradiating a target tissue is approximately equal to the SAF when the source and target designations are reversed (Cristy and Eckerman, 1987).

Scaling of reference cross-dose SAFs to estimate non-reference cross-dose SAFs was performed by interpolating between the full set of SAFs generated through the sphere simulations. The SAF set was a function of initial energy, source size, target size, and source-target separation. Initial energies of all radiation energies in a given spectrum are known, so energy interpolation can be performed. Next, the reference source size, target size, and source-target separation is used to interpolate an equivalent reference SAF from the sphere-based dataset. The equivalent non-reference SAF is interpolated from the sphere-based dataset based on the non-reference source size, target size, and source-target separation. The ratio of the equivalent non-reference SAF and equivalent reference SAF is calculated and then applied to the actual reference SAF for the source-target-energy combination of interest.

The cross-dose study was not repeated for electrons because it was hypothesized that results for electrons would be insufficient for two reasons – (1) poor statistical uncertainties at the defined center-to-center separations and (2) no primary electron dose contributions at any of the center-to-center separations. Since primary (collisional energy loss mechanisms) electron dose contributions depend heavily on the surface shape and surface-to-surface distance of the source and target tissues, the primary electron dose contribution would be problematic to scale since modeling surface-to-surface distances in the clinic is prohibitively difficult. Considering this, the photon cross-dose

scaling methods were applied only to the radiative component of the electron dose during the validation studies.

2.2.2 Cross-Dose Validation Studies The cross-dose validation study was performed using the same methodology as the self-dose validation study detailed above. Cross-dose from the liver irradiating the spleen was calculated for each CT image-based patient-specific phantom. The relevant reference phantom (e.g., the UFHADM reference phantom for an adult male patient-specific phantom) liver-to-spleen cross-dose SAFs published in Wayson (2012) were scaled using the interpolated scaling factors detailed in Section 2.2.1 as a function of radiation energy and source/target tissue size and separation. The scaled SAFs were used to calculate the reference-scaled S value. This scaled S value was then compared to the liver-to-spleen cross-dose S value obtained from the patient-specific MCNPX v2.6 simulations discussed above.

3. Results

3.1 Photon Self-Dose

Results for photon self-dose SAFs at all sphere masses and photon energies are shown in Figure 1. Statistical uncertainties were less than 0.1% for all sphere sizes due to the large number of interactions in the source tissue. SAF variations are seen with both initial photon energy and sphere size. This suggests that the power R used for photon self-dose scaling should depend on both the initial photon energy and sizes of the reference and non-reference spheres. Photon self-dose SAFs decrease with increasing sphere size because the increase in sphere mass dominates the increase in self-absorption, recalling that the SAF is the absorbed fraction divided by the target mass. The SAF increase at lower energies is due to increased photoelectric absorption, and the decrease at higher energies is due to more secondary electrons escaping as they attain greater initial kinetic energies.

More variation with energy is observed for smaller sphere sizes because a larger fraction of secondary electron escape when the overall dimensions of the sphere is smaller.

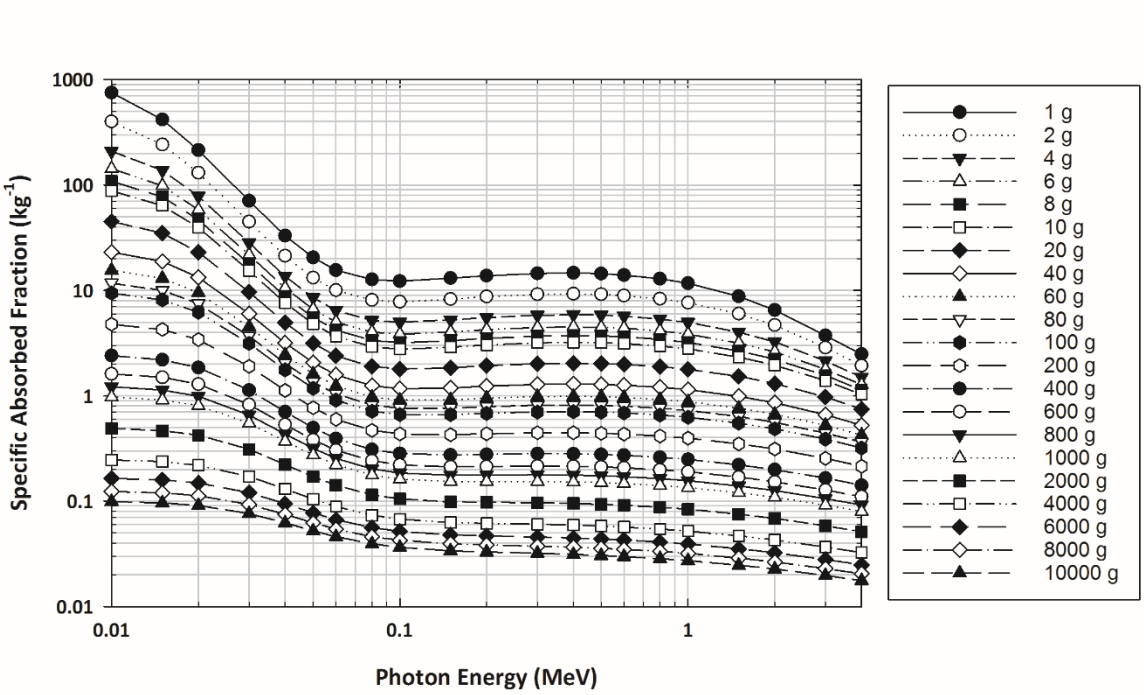

Figure 1. Sphere self-dose SAFs as a function of initial photon energy and sphere size for the photon self-dose scaling study.

Results for the computed mass ratio scaling power R as a function of initial photon energy and reference sphere mass are shown in Figure 2 averaged over the non-reference sphere size. The scaling power is dependent on the initial photon energy with widely varying values for energies less than 100 keV and greater than 1 MeV. An 18% percent difference between the scaling powers of the 1 g and 10 kg reference spheres was observed at 30 keV, and a 37% difference was observed at 4 MeV between the same reference sphere sizes.

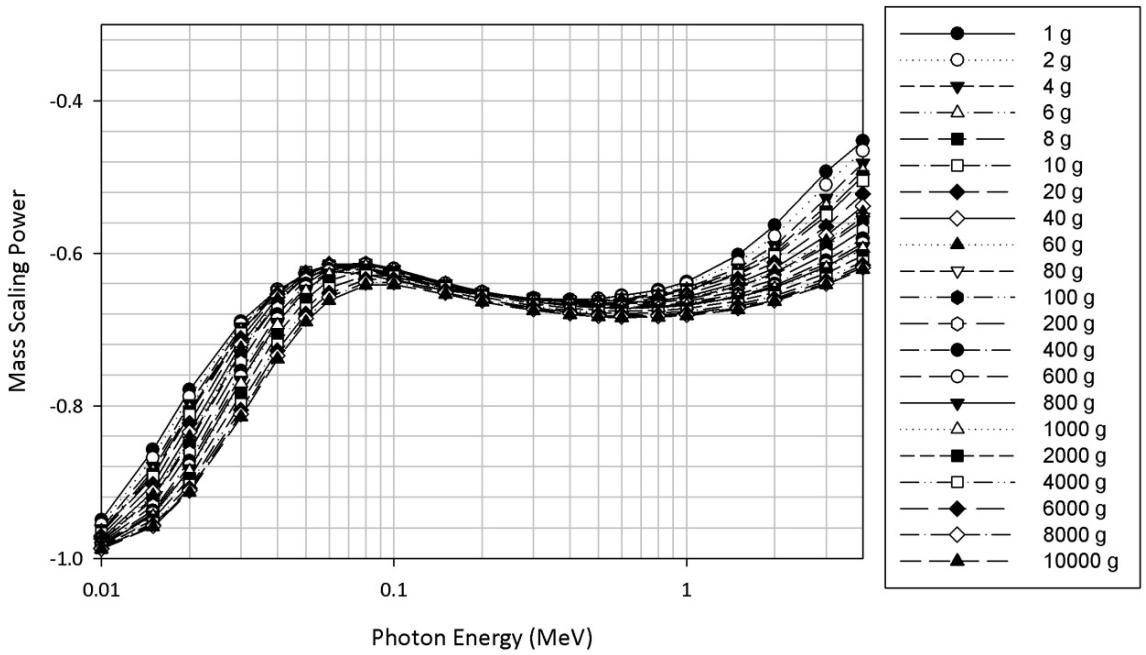

Figure 2. Mass ratio scaling powers for photon self-dose as a function of both reference sphere mass and initial photon energy. Results are averaged over non-reference sphere size.

3.2 Electron Self-Dose

Electron self-dose SAFs can be seen in Figure 3. Energy dependence is demonstrated by the downward tilt of many SAF curves beginning around 300 keV. Mass dependence is demonstrated by the varying curve shapes of the different sphere sizes. Electron self-dose SAFs decrease with increasing sphere size because the target mass dominates the SAF equation. The results suggest that energy- and mass-independent scaling methodologies for electron self-dose may not be sufficient to accurately account for electron escape and photon production at higher electron energies. When electron initial kinetic energies are relatively low, most of the energy is locally deposited. At higher energies, electrons attain sufficient energy to escape the sphere and produce more bremsstrahlung x-rays that carry off some of that initial kinetic energy. Energy escape is more prominent for smaller sphere sizes because the smaller overall dimensions of the sphere allow for greater escape.

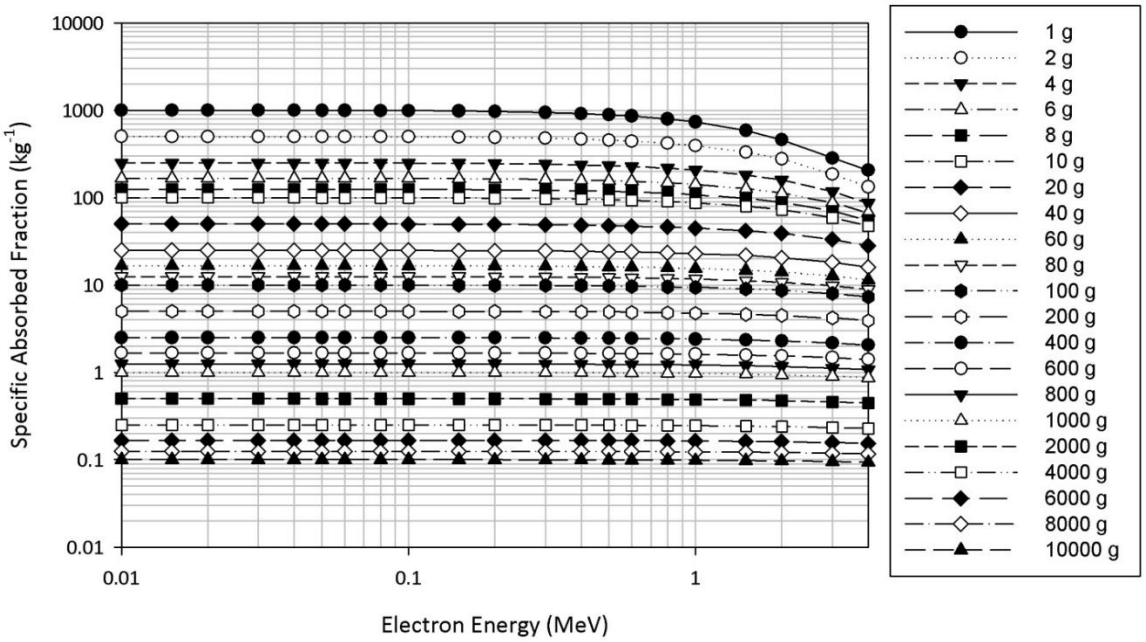

Figure 3. Sphere self-dose SAFs as a function of initial electron energy and sphere size for the electron self-dose scaling study.

Electron self-dose mass ratio scaling powers R averaged over non-reference sphere size are shown in Figure 4. Energy dependence becomes evident at electron energies around 300 keV as electron escape becomes significant. In addition, electron self-dose scaling powers should vary as a function of mass. A 27% percent difference between the mass scaling powers of the 1 g and 10 kg spheres was observed at 4 MeV. Electron self-dose AFs do not remain close to unity at high energies and small sphere sizes.

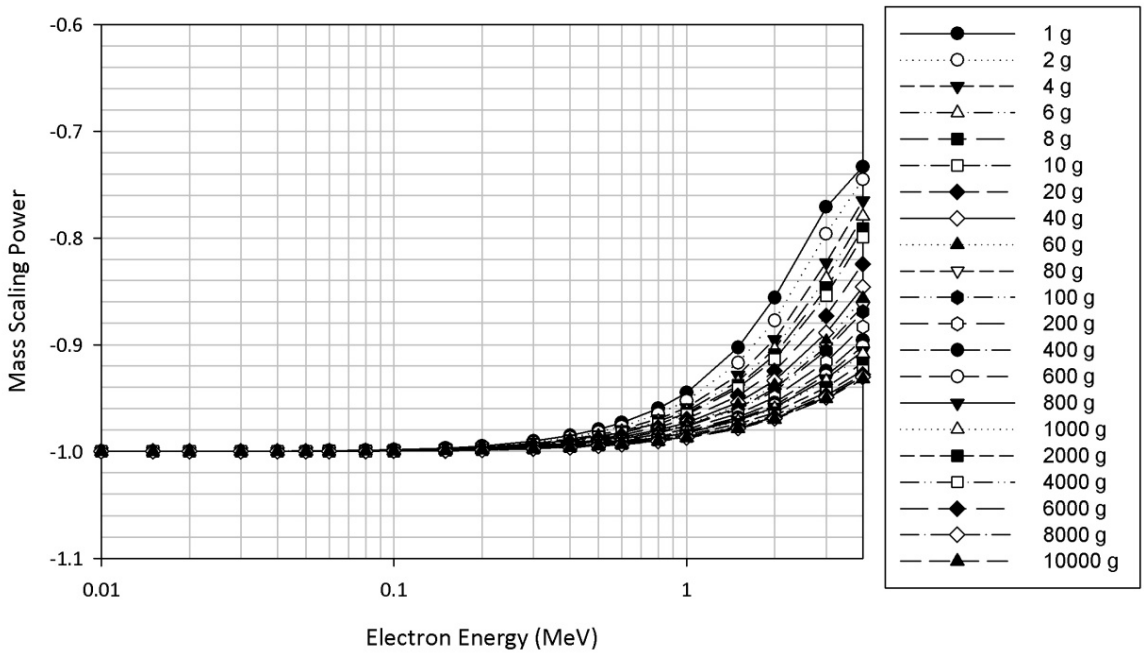

Figure 4. Mass ratio scaling powers for electron self-dose as a function of both reference sphere mass and initial electron energy. Results are averaged over non-reference sphere size.

3.3 Photon Cross-Dose

Next, dosimetric trends were investigated for photon cross-dose, recalling the irradiation geometry of varying sizes of concentric spheres. Figure 5 illustrates variations of SAFs as a function of both the separation distance between the source and target sphere mass with sub-figures (A), (B), and (C) indicating changes in these relationships with varying source sphere masses. In each sub-figure, the dominant dependence is on center-to-center separation. This is expected due to inverse square law and attenuation effects.

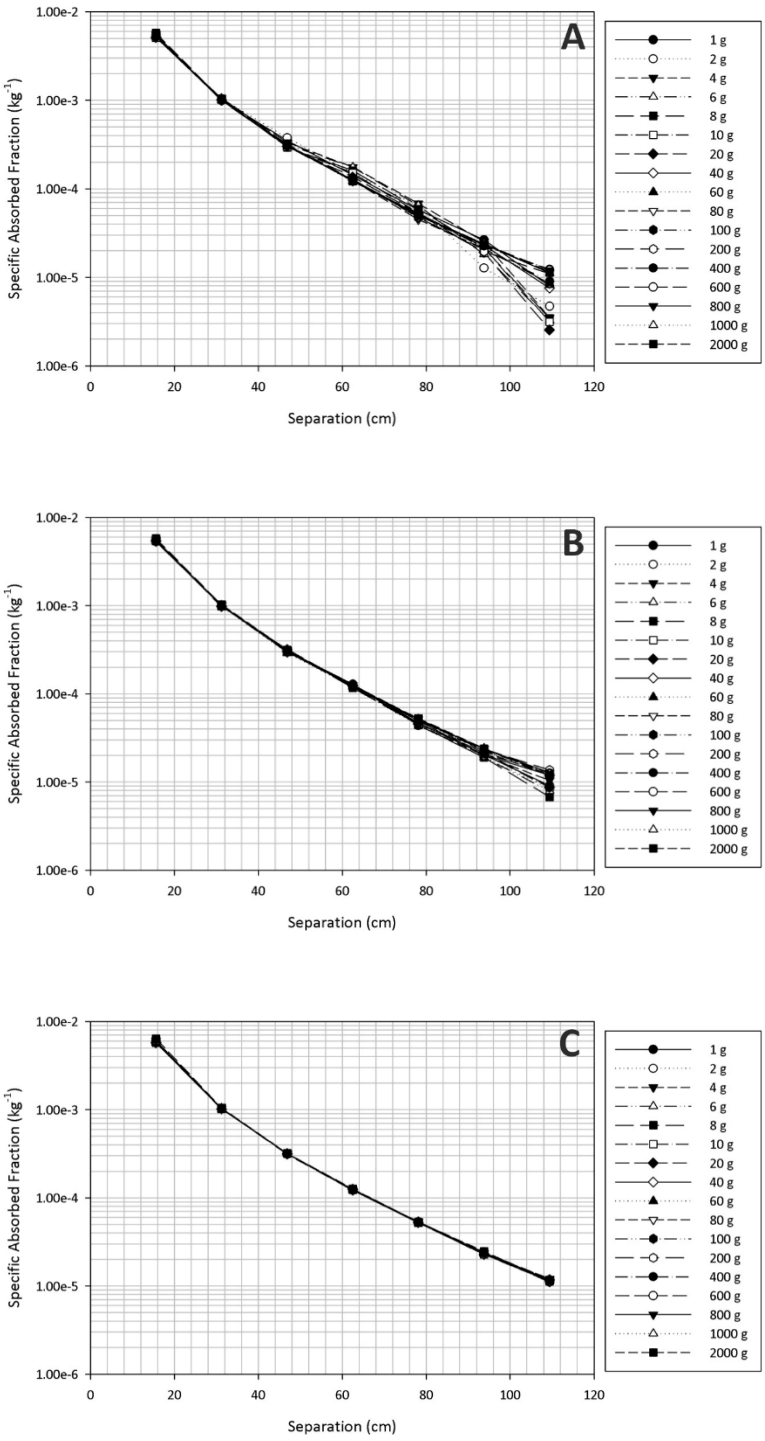

Figure 5. Photon specific absorbed fractions for the (A) 1 g, (B) 100 g, and (C) 2 kg source spheres and 4 MeV photons as a function of sphere separation and target sphere mass.

From Figure 5A, it is unclear at first glance whether the difference in SAFs at the largest separation is due to real differences in dose or to statistical uncertainties at that particular irradiation geometry (4 MeV photon energy and 1 g source mass). The average statistical uncertainty for that irradiation geometry is 32.8% (range of 4.5% to 99.6%) which is considered to be unreliable. However, statistical uncertainties at the first two (and possibly third) separations were considered reliable at average uncertainties of 5.0%, 8.4%, and 11.5%, respectively. Predictably, as the source mass increased, the variations in the SAF were minimized, a result of the statistical uncertainty effects of reverse Monte Carlo techniques. As the source sphere increased in size, more interactions occurred in the target sphere for the reverse Monte Carlo designation (e.g., the final retained SAFs for the 2 kg sphere irradiating the 1 g sphere were actually the SAFs for the 1 g sphere irradiating the 2 kg sphere).

At the largest source mass, no clear trends exist for dose differences with variations in target mass size at large distances (Figure 5C). Target mass size independence is also observed across photon energies (Figure 6). Across the first six source-target separation distances and all target spheres, an average of 12% difference was seen between the maximum and minimum SAFs at each source-target separation distance and target sphere size. Qualitatively, it is clear that no appreciable trend exists for variations in target dose as a function of source size.

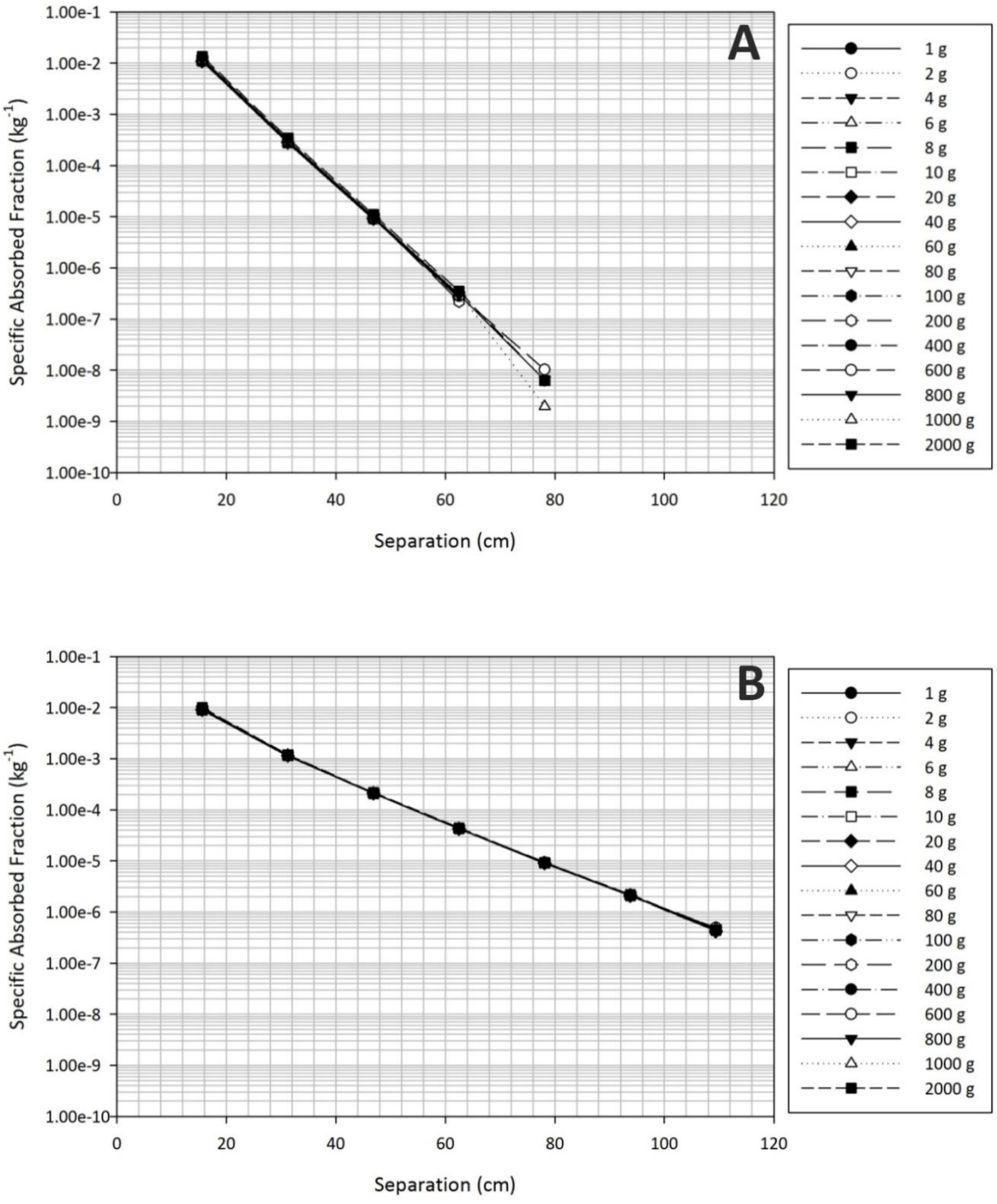

Figure 6. Photon specific absorbed fractions for the 2 kg source spheres and (A) 50 keV and (B) 500 keV photons as a function of sphere separation and target sphere mass (the 4 $MeV - 2\ kg$ source sphere irradiation geometry can be seen in Figure 5 for comparison).

The photon cross-dose SAF curves mostly showed that SAFs for a given source sphere size and separation did not vary with target sphere size. This was expected since the reduction in target sphere mass was accompanied by a reduction in absorbed energy. However, results for the $4\ MeV - 2\ kg$ source sphere irradiation geometry in Figure 5 seemed to indicate that this target size independence begins to break down at the $15.63\ cm$ source-target separation. The difference between the minimum and maximum SAFs (varying with target sphere size) for a $2\ kg$ source sphere for $4\ MeV$ photons was 4% for the 5th ($78.16\ cm$) separation and 11% for the 1st ($15.63\ cm$) separation. This suggests that the SAFs begin to diverge for different target sphere sizes at a separation around $15\ cm$. Since statistical uncertainties associated with the SAFs at the $15.63\ cm$ separation were all less than 4%, the increased SAF difference was likely due to actual differences in SAFs rather than to statistical uncertainties.

Figure 7 shows photon SAFs as a function of sphere separation, target mass, and source mass for $4\ MeV$ photons in the close-to-mid-range distance simulations. Additionally, Figure 8 shows photon SAFs as a function of separation, target mass, and photon energy for the $20\ g$ source sphere. For higher energies, even at these close separations, the SAF does not vary considerably as a function of source or target mass. However, Figure 8 gives evidence that dose scaling may be necessary for low energies, even for larger source masses. At each photon energy, separation, and source size, the minimum and maximum SAFs were compared across all target sizes. On average, the maximum SAF was 2.9% greater than the minimum SAF for energies $50\ keV$ or greater but 340% greater for energies less than $50\ keV$. These results at low energies and close separations require the possibility of mass-based dose-scaling methods for photon cross-dose.

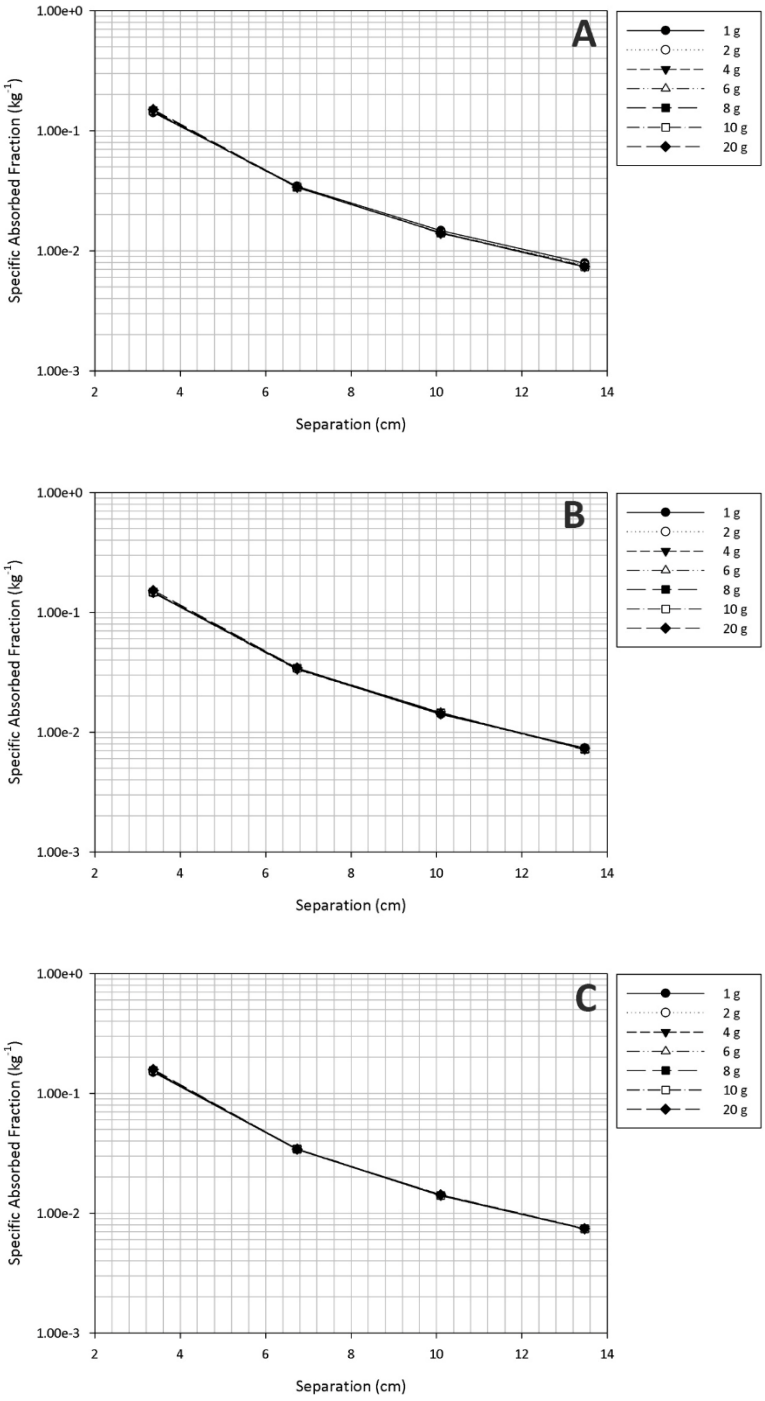

Figure 7. Photon specific absorbed fractions for the (A) 1 g, (B) 6 g, and (C) 20 g (following page) source spheres and 4 MeV photons as a function of sphere separation and target sphere mass.

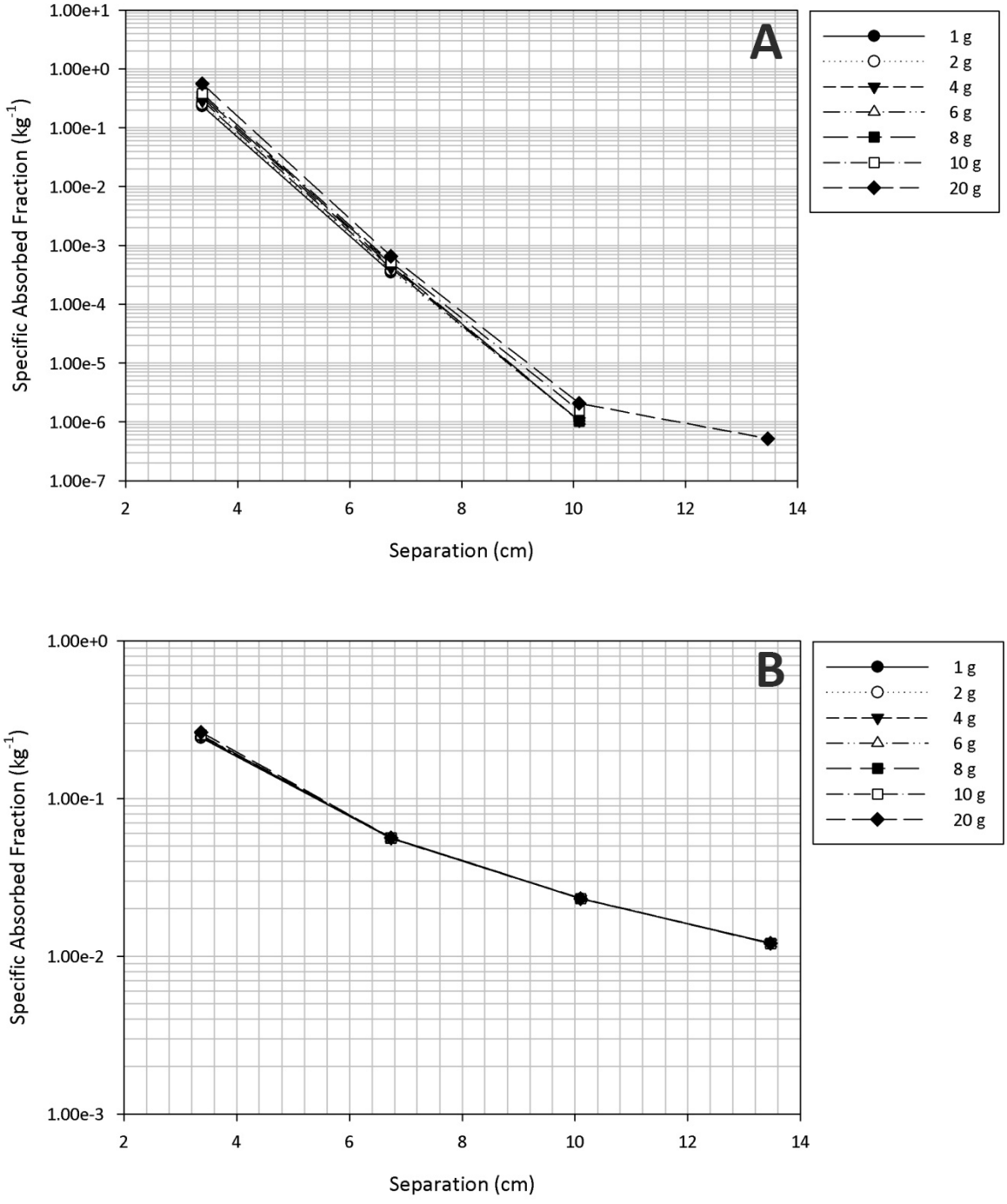

Figure 8. Photon specific absorbed fractions for the 20 g source spheres and (A) 15 keV and (B) 500 keV photons as a function of sphere separation and target sphere mass.

3.4 Electron Cross-Dose

The close-to-mid-separation simulation set was also performed for electrons. Distant separations were not simulated for electrons because it was assumed that statistical uncertainties would be too poor to generate meaningful results. Results similar in format to those of the photon cross-dose analysis are shown in Figures 9 and 10. Figure 9 shows that differences in electron SAFs at more distant center-to-center separations mimic those seen in the photon cross-dose simulations. However, at the closest separation of 3.37 cm, differences by orders of magnitude appear between the minimum and maximum SAFs of the different target sphere sizes, presumably due to varying levels of primary electron dose contributions. Figure 10 seems to corroborate this assumption as most SAFs follow the photon trend for the 50 keV and 500 keV electron energies with the one exception being the 20 g target tissue at 3.37 cm separation for 500 keV electrons.

To further investigate the nature of electron SAF variations with changes in source and target tissues, SAFs as a function of initial electron energy and target tissue size are shown for the 20 g source tissue and 3.37 cm separation in Figure 11. As noted when discussing the monoenergetic electron SAFs, these curves all show collisional energy loss characteristics. The surface of each target sphere is located at a different distance from the source sphere despite the constant center-to-center separation. Primary electrons interact with the largest target sphere first, so the dose to the largest target sphere is greater than each subsequently smaller target sphere. This trend can be observed in Figure 11 at electron energies 1 MeV and greater.

Primary electron cross-dose scaling may be impractical to address since surface shape and surface separation affect the dose estimate much more than for photons. Electron cross-dose contributions from radiative losses, on the other hand, can be handled in the same way as the photon cross-dose simulations, and results show that distance scaling may be a viable option.

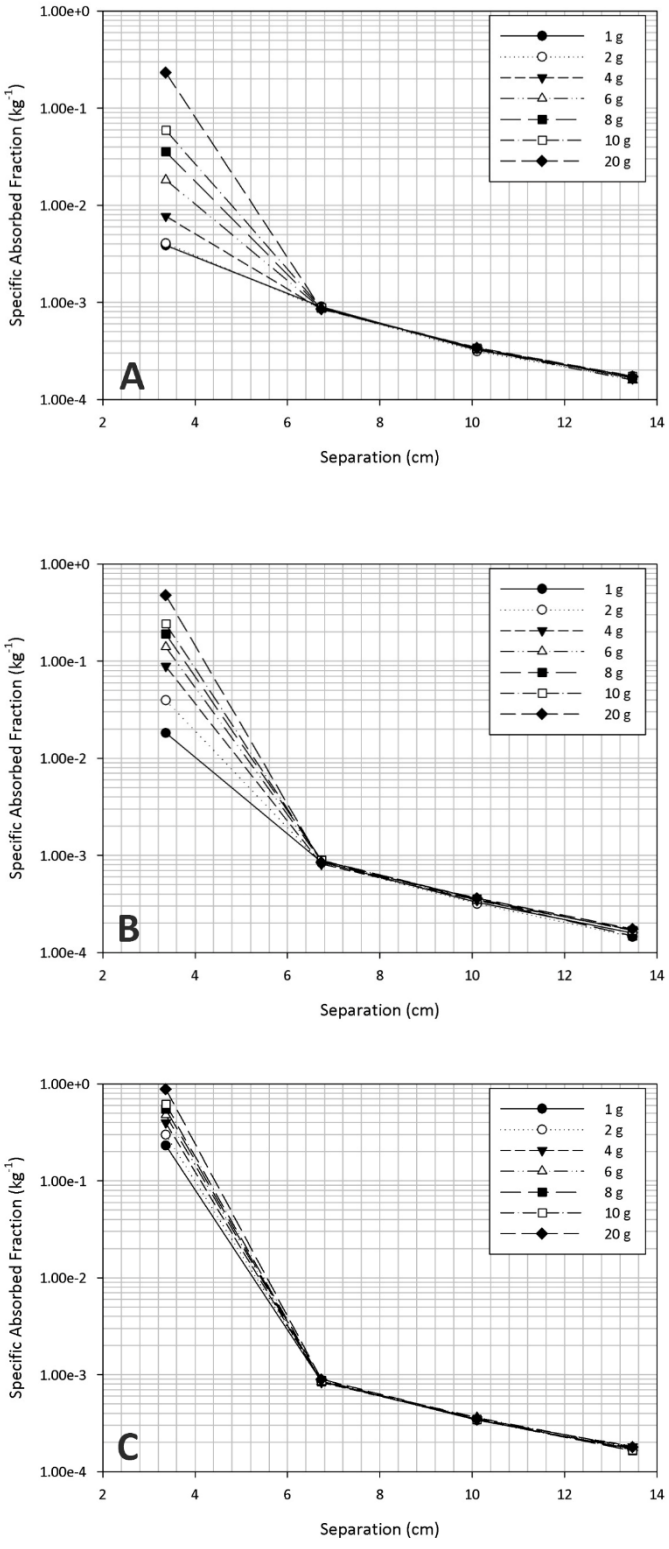

Figure 9. Electron specific absorbed fractions for the (A) 1 g, (B) 6 g, and (C) 20 g (following page) source spheres and 4 MeV electrons as a function of sphere separation and target sphere mass.

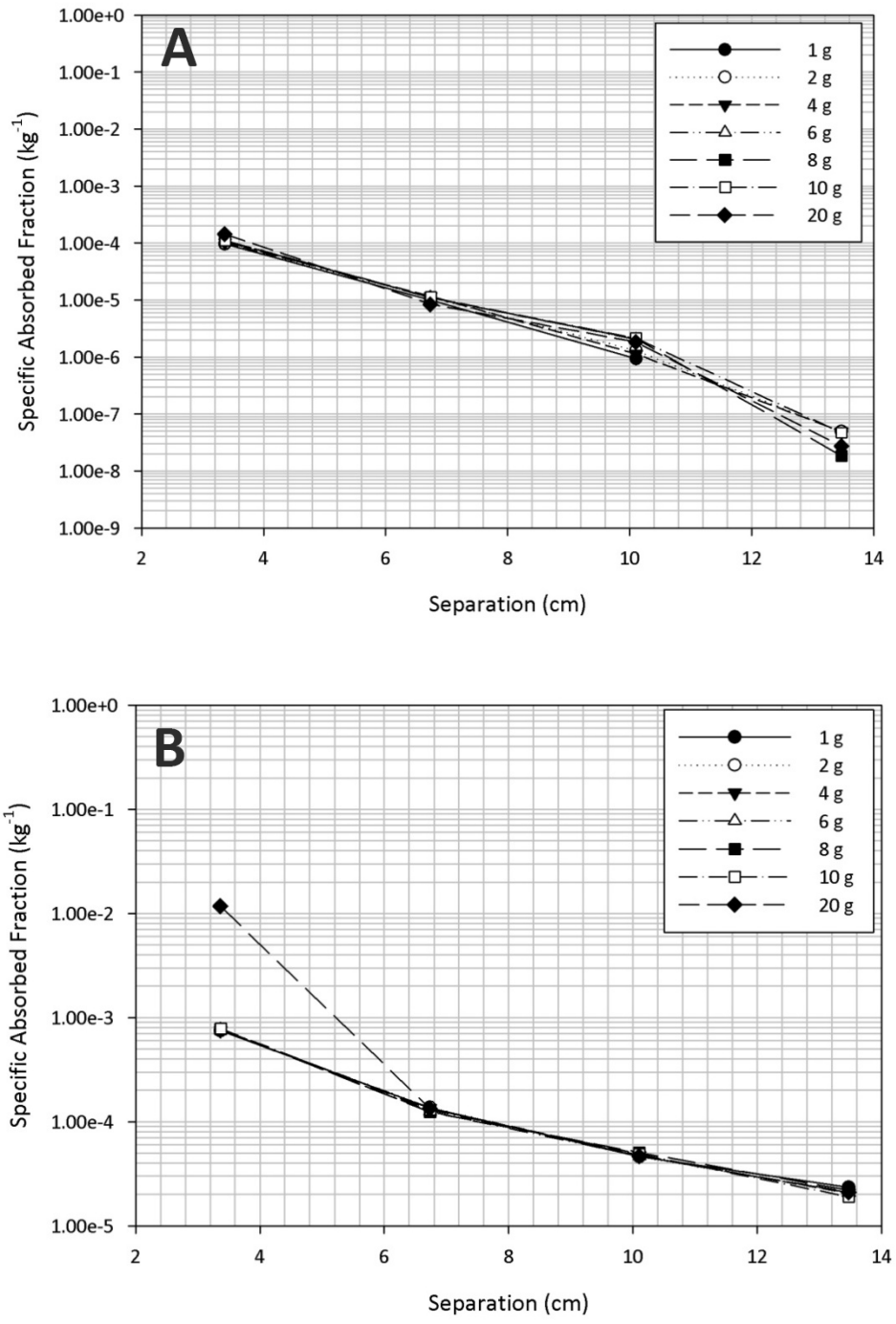

Figure 10. Electron specific absorbed fractions for the 20 g source spheres and (A) 50 keV and (B) 500 keV electrons as a function of sphere separation and target sphere mass.

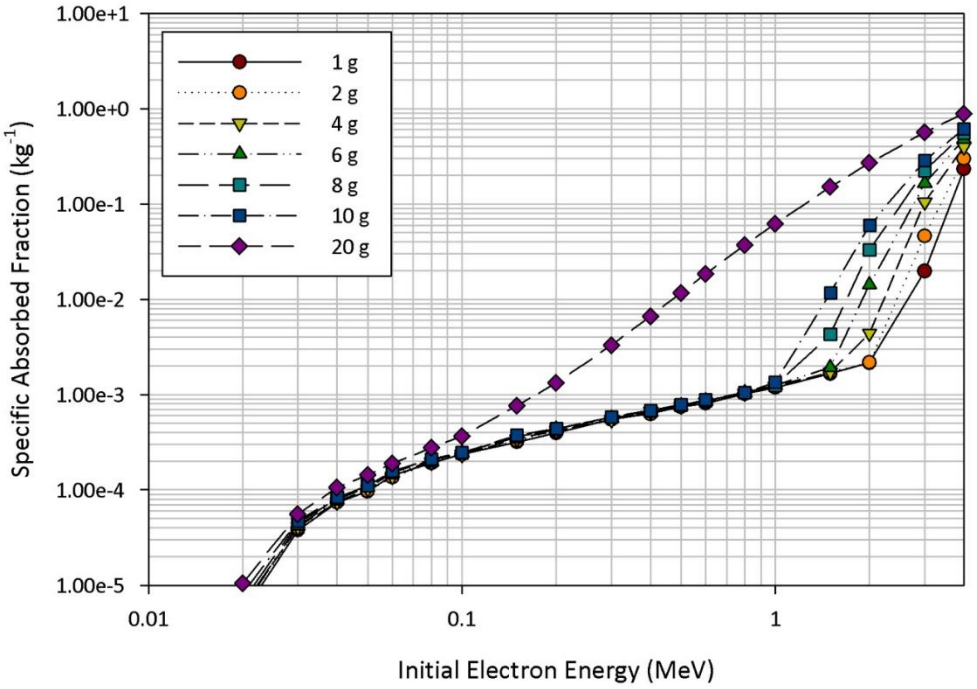

Figure 11. Electron cross-dose SAFs for differing target sphere sizes for the 3.37 *cm* center-to-center separation and 20 *g* source sphere.

4. Discussion

4.1 Photon Self-Dose

An improvement over the MIRD 11 recommendation can be achieved by applying the apparent energy and mass dependence of the mass ratio scaling power R. The recommendation to apply a scaling power of $-2/3$ seems only appropriate for a relatively narrow photon energy range (200 – 400 keV), and not completely representative of the tendencies at lower and higher photon energies (Snyder *et al.*, 1975).

A 3D matrix of self-dose scaling power R was developed as a function of photon energy, reference sphere size, and non-reference sphere size. A sample of this 3-D matrix showing scaling powers for 4 MeV photons can be seen in Table 2. For example, referencing Table 2, if the reference

tissue mass was 60 g and the non-reference tissue mass was 80 g, the non-reference SAF would be computed as:

$$\Phi(r_T \leftarrow r_S, 4\ MeV, 80\ g) = \Phi(r_T \leftarrow r_S, 4\ MeV, 60\ g)\left(\frac{80\ g}{60\ g}\right)^{-0.548} \quad (5)$$

In this example, the SAF for the non-reference, larger sphere is obtained by multiplying the reference SAF by a factor of 0.854. This is expected because previously studied dosimetric trends predict that the photon self-dose SAF decreases with increasing tissue mass (Petoussi-Henss *et al.*, 2007). For practical applications within an internal dosimetry software, 3D interpolation would be performed to obtain mass ratio scaling powers unique to the reference mass, non-reference mass, and photon energy of interest.

The set of patient-specific phantoms were used to compare the UF and MIRD photon self-dose scaling methods. The UF method of self-dose scaling utilized the scaling factors developed in the current work. Uniform ^{131}I photon sources were simulated in the liver and spleen of 14 male and 13 female patient-specific phantoms. The results of this validation study are in Table 3 and show the deviation between the patient-specific simulated S value and the scaled S value computed using scaled SAFs. The MIRD and UF self-dose scaling methods are both good at predicting dose changes for the given set of patient-specific phantoms. The average gain in accuracy between the two methods is well below 1% for the ^{131}I photon spectrum. The principle photon emission energy for ^{131}I is 364 keV, and so the MIRD and UF method tend to converge for this particular application.

Table 2. Excerpt of the 3D mass ratio scaling power matrix used to scale photon self-dose showing results for 4 MeV photons.

	Sphere Mass (g)									
Sphere Mass (g)	1	4	8	10	40	80	100	400	800	1000
1	--	-0.365	-0.379	-0.384	-0.421	-0.440	-0.446	-0.478	-0.493	-0.498
2	-0.360	-0.371	-0.389	-0.394	-0.435	-0.455	-0.461	-0.494	-0.509	-0.513
4	-0.365	--	-0.406	-0.411	-0.455	-0.474	-0.480	-0.513	-0.527	-0.531
6	-0.373	-0.398	-0.417	-0.422	-0.467	-0.486	-0.492	-0.524	-0.537	-0.541
8	-0.379	-0.406	--	-0.429	-0.476	-0.495	-0.500	-0.531	-0.545	-0.549
10	-0.384	-0.411	-0.429	--	-0.483	-0.502	-0.507	-0.538	-0.551	-0.555
20	-0.402	-0.433	-0.453	-0.461	-0.506	-0.522	-0.528	-0.555	-0.567	-0.571
40	-0.421	-0.455	-0.476	-0.483	--	-0.539	-0.544	-0.570	-0.582	-0.585
60	-0.432	-0.466	-0.487	-0.494	-0.532	**-0.548**	-0.553	-0.579	-0.589	-0.593
80	-0.440	-0.474	-0.495	-0.502	-0.539	--	-0.559	-0.584	-0.595	-0.598
100	-0.446	-0.480	-0.500	-0.507	-0.544	-0.559	--	-0.588	-0.598	-0.602
200	-0.463	-0.497	-0.517	-0.524	-0.559	-0.573	-0.578	-0.598	-0.609	-0.612
400	-0.478	-0.513	-0.531	-0.538	-0.570	-0.584	-0.588	--	-0.619	-0.623
600	-0.487	-0.521	-0.539	-0.545	-0.577	-0.590	-0.594	-0.613	-0.629	-0.631
800	-0.493	-0.527	-0.545	-0.551	-0.582	-0.595	-0.598	-0.619	--	-0.635
1000	-0.498	-0.531	-0.549	-0.555	-0.585	-0.598	-0.602	-0.623	-0.635	--
2000	-0.511	-0.543	-0.560	-0.566	-0.595	-0.607	-0.611	-0.630	-0.639	-0.640
4000	-0.523	-0.554	-0.571	-0.576	-0.604	-0.615	-0.619	-0.637	-0.645	-0.647
6000	-0.529	-0.560	-0.577	-0.582	-0.609	-0.620	-0.624	-0.642	-0.649	-0.651
8000	-0.534	-0.564	-0.580	-0.585	-0.612	-0.623	-0.627	-0.644	-0.652	-0.654
10000	-0.537	-0.568	-0.583	-0.588	-0.615	-0.626	-0.629	-0.646	-0.654	-0.656

Table 3. Patient-specific photon self-dose scaling validation study using all UF mass ratio scaling powers for ^{131}I photons. The patient-specific naming convention is [gender][height in centimeters][weight in kilograms] (e.g., m-193-132 is a 193 cm tall, 132 kg male). Deviation percentage is relative to the explicitly simulated patient-specific model.

	UF deviation (%)		MIRD deviation (%)		Preferred method		Percentage point gain (%)	
Phantom	Liver	Spleen	Liver	Spleen	Liver	Spleen	Liver	Spleen
Male								
m-193-132	1.9	0.6	2.8	0.9	UF	UF	0.9	0.3
m-183-120	0.6	0.7	0.1	0.6	MIRD	MIRD	0.5	0.1
m-183-112	1.6	1.9	1.8	1.7	UF	MIRD	0.2	0.2
m-183-86	5.3	1.3	5.3	1.3	MIRD	UF	0.0	0.0
m-180-82	1.4	0.1	1.7	0.1	UF	UF	0.3	0.0
m-178-100	0.9	0.1	1.2	0.2	UF	UF	0.3	0.1
m-178-73	6.5	0.2	6.5	0.5	MIRD	UF	0.0	0.3
m-175-81	2.2	5.7	2.2	5.8	UF	UF	0.0	0.1
m-175-66	5.2	1.7	5.1	1.9	MIRD	UF	0.1	0.2
m-173-98	2.9	2.1	2.8	2.0	MIRD	MIRD	0.1	0.1
m-173-74	0.8	0.7	1.0	0.5	UF	MIRD	0.2	0.2
m-168-78	1.9	4.9	1.4	4.8	MIRD	MIRD	0.5	0.1
m-165-74	0.6	0.5	0.5	0.7	MIRD	UF	0.1	0.2
m-157-44	3.8	4.7	3.1	4.5	MIRD	MIRD	0.7	0.2
Female								
f-164-59	5.1	13.3	4.8	13.2	MIRD	MIRD	0.3	0.1
f-175-136	0.7	8.6	0.2	8.8	MIRD	UF	0.5	0.2
f-173-82	4.5	11.4	4.2	11.5	MIRD	UF	0.3	0.1
f-165-63	0.4	10.1	0.7	9.8	UF	MIRD	0.3	0.3
f-163-117	3.2	7.3	2.0	7.6	MIRD	UF	1.2	0.3
f-163-80	2.0	6.9	1.6	7.0	MIRD	UF	0.4	0.1
f-160-61	2.3	10.9	2.2	10.7	MIRD	MIRD	0.1	0.2
f-160-52	0.9	5.2	0.5	5.0	MIRD	MIRD	0.4	0.2
f-160-51	4.6	5.6	4.4	5.8	MIRD	UF	0.2	0.2
f-155-98	3.9	7.4	3.8	7.3	MIRD	MIRD	0.1	0.1
f-155-70	0.7	0.4	0.5	0.7	MIRD	UF	0.2	0.3
f-155-48	2.2	6.2	2.1	6.2	MIRD	UF	0.1	0.0
f-152-66	3.2	6.4	3.3	6.6	UF	UF	0.1	0.2

4.2 Electron Self-Dose

Mass ratio scaling powers R were again used as the basis for dose scaling for electron self-dose. A 3D matrix of scaling powers was developed as a function of electron energy, source size, and target size. A sample of this 3D matrix showing scaling powers for4 MeV electrons can be seen in Table 4. As an example, if the reference tissue mass was 20 g and the non-reference tissue mass was 40 g, the non-reference SAF would be computed as:

$$\Phi(r_T \leftarrow r_S, 4\ MeV, 40\ g) = \Phi(r_T \leftarrow r_S, 4\ MeV, 20\ g)\left(\frac{40\ g}{20\ g}\right)^{-0.809} \quad (6)$$

In this example, the SAF for the non-reference, larger sphere is obtained by multiplying the reference SAF by a factor of 0.571. This is expected because previously studied dosimetric trends predict that the electron self-dose SAF decreases with increasing tissue mass (ICRP, 1980). For practical applications within internal dosimetry software, 3D interpolation would be performed to obtain mass ratio scaling powers unique to the reference mass, non-reference mass, and electron energy of interest.

Table 4. Excerpt of the 3-D mass ratio scaling power matrix used to scale electron self-dose showing results for 4 MeV electrons.

	Sphere Mass (g)									
Sphere Mass (g)	1	4	8	10	40	80	100	400	800	1000
1	--	-0.626	-0.633	-0.640	-0.691	-0.717	-0.725	-0.769	-0.787	-0.792
2	-0.632	-0.620	-0.634	-0.643	-0.705	-0.734	-0.742	-0.787	-0.805	-0.810
4	-0.626	--	-0.649	-0.660	-0.731	-0.760	-0.768	-0.812	-0.829	-0.834
6	-0.628	-0.636	-0.667	-0.680	-0.751	-0.779	-0.787	-0.829	-0.845	-0.849
8	-0.633	-0.649	--	-0.696	-0.766	-0.793	-0.801	-0.841	-0.856	-0.860
10	-0.640	-0.660	-0.696	--	-0.777	-0.804	-0.811	-0.849	-0.864	-0.868
20	-0.664	-0.697	-0.733	-0.745	**-0.809**	-0.833	-0.840	-0.874	-0.886	-0.890
40	-0.691	-0.731	-0.766	-0.777	--	-0.857	-0.863	-0.893	-0.904	-0.908
60	-0.707	-0.748	-0.782	-0.793	-0.848	-0.869	-0.874	-0.903	-0.913	-0.916
80	-0.717	-0.760	-0.793	-0.804	-0.857	--	-0.881	-0.909	-0.919	-0.922
100	-0.725	-0.768	-0.801	-0.811	-0.863	-0.881	--	-0.913	-0.923	-0.925
200	-0.748	-0.792	-0.823	-0.832	-0.879	-0.897	-0.902	-0.925	-0.933	-0.936
400	-0.769	-0.812	-0.841	-0.849	-0.893	-0.909	-0.913	--	-0.942	-0.944
600	-0.780	-0.822	-0.850	-0.858	-0.900	-0.915	-0.919	-0.939	-0.946	-0.948
800	-0.787	-0.829	-0.856	-0.864	-0.904	-0.919	-0.923	-0.942	--	-0.951
1000	-0.792	-0.834	-0.860	-0.868	-0.908	-0.922	-0.925	-0.944	-0.951	--
2000	-0.807	-0.848	-0.873	-0.880	-0.917	-0.930	-0.933	-0.950	-0.957	-0.959
4000	-0.821	-0.860	-0.883	-0.890	-0.924	-0.936	-0.940	-0.956	-0.961	-0.963
6000	-0.828	-0.866	-0.889	-0.895	-0.928	-0.940	-0.943	-0.958	-0.964	-0.965
8000	-0.832	-0.870	-0.892	-0.899	-0.931	-0.942	-0.945	-0.960	-0.965	-0.967
10000	-0.836	-0.873	-0.895	-0.901	-0.933	-0.944	-0.947	-0.961	-0.966	-0.968

The same self-dose validation studies performed for photons were also performed for electrons. Results for the uniform ^{90}Y beta sources in the liver and spleen of the 14 adult male and 13 adult female patient-specific phantoms are given in Table 5 showing the deviation between the patient-specific simulated S value and the scaled S value computed using scaled SAFs. Electron self-dose scaling results mirrored those of the photons sources. Both the MIRD and UF methods performed well at predicting the non-reference S values. The UF method performed slightly better for the smaller source organ (spleen), while the MIRD method performed slightly better for the larger source organ (liver). Greater gains in accuracy were achieved with the UF method for the smaller source organs. At sufficiently high electron energies and for smaller source sizes, the electron AF deviates significantly from unity, and it is in these cases where the UF method would provide improvements in patient-specific dose estimates.

Table 5. Patient-specific electron self-dose scaling validation study using all UF mass ratio scaling powers for ^{90}Y beta particles. The patient-specific naming convention is [gender][height in centimeters][weight in kilograms] (e.g., m-193-132 is a 193 cm tall, 132 kg male). Deviation percentage is relative to the explicitly simulated patient-specific model.

	UF deviation (%)		MIRD deviation (%)		Preferred method		Percentage point gain (%)	
Phantom	Liver	Spleen	Liver	Spleen	Liver	Spleen	Liver	Spleen
Male								
m-193-132	0.8	0.4	0.3	1.9	MIRD	UF	0.5	1.5
m-183-120	0.8	0.5	0.4	2.3	MIRD	UF	0.4	1.8
m-183-112	0.9	1	0.8	0.5	MIRD	MIRD	0.1	0.5
m-183-86	1.3	0.2	1.3	3	UF	UF	None	2.8
m-180-82	0.9	1.3	0.7	0.9	MIRD	MIRD	0.2	0.4
m-178-100	0.8	0.2	0.6	3.2	MIRD	UF	0.2	3.0
m-178-73	1.3	0.4	1.3	1.7	UF	UF	None	1.3
m-175-81	0.8	0.1	0.7	0.9	MIRD	UF	0.1	0.8
m-175-66	1.4	0.5	1.4	1.3	UF	UF	None	0.8
m-173-98	0.6	1.1	0.5	0	MIRD	MIRD	0.1	1.1
m-173-74	0.8	1.5	0.9	2.9	UF	UF	0.1	1.4
m-168-78	1.2	1.9	1.7	1.3	UF	MIRD	0.5	0.6
m-165-74	0.9	0.8	0.9	0.2	UF	MIRD	None	0.6
m-157-44	1.3	1.6	2.2	1.2	UF	MIRD	0.9	0.4
Female								
f-164-59	0.5	1.1	0.2	0.3	MIRD	MIRD	0.3	0.8
f-175-136	0.8	0.6	0.4	2	MIRD	UF	0.4	1.4
f-173-82	0.5	1.1	0.1	2.1	MIRD	UF	0.4	1.0
f-165-63	1.3	0.3	1.6	1.5	UF	UF	0.3	1.2
f-163-117	0.5	1.1	0.3	3.8	MIRD	UF	0.2	2.7
f-163-80	0.6	0.3	0.3	1.1	MIRD	UF	0.3	0.8
f-160-61	0.7	0.7	0.7	0.3	MIRD	MIRD	None	0.4
f-160-52	1.3	0.6	1.7	1.4	UF	UF	0.4	0.8
f-160-51	1.1	0	1.2	1	UF	UF	0.1	1.0
f-155-98	0.9	0.2	0.9	0.6	MIRD	UF	None	0.4
f-155-70	0.8	1.1	0.5	0.5	MIRD	MIRD	0.3	0.6
f-155-48	0.7	0	0.7	0.3	MIRD	UF	None	0.3
f-152-66	1.4	0.4	1.3	1.7	MIRD	UF	0.1	1.3

4.3 Photon Cross-Dose

Instead of using mass ratio scaling powers for the photon cross-dose scaling methodology, SAF ratios were used to scale reference cross-dose SAFs based on inputs of reference and non-reference center-to-center separations, reference source and target masses, non-reference source and target masses, and radionuclide emission energies. An excerpt of the photon cross-dose tables can be seen in Table 6. The full dataset contains 17 source sizes, 17 target sizes, 7 center-to-center separations, and 21 photon energies.

To illustrate how the photon cross-dose sphere SAFs were utilized, consider an arbitrary reference irradiation geometry where the source tissue is 1.00 g, the target tissue is 2.00 g, the center-to-center separation is 15.6 cm, and the photon energy is 4 MeV. The non-reference source tissue mass, target tissue mass, center-to-center separation, and photon energy are 2.00 g, 4.00 g, 31.3 cm, and 4 MeV, respectively. The equivalent reference sphere SAF is $5.22 \times 10^{-3}\ kg^{-1}$, and the equivalent non-reference sphere SAF is $1.09 \times 10^{-3}\ kg^{-1}$. To obtain the predicted non-reference SAF, the reference SAF would be multiplied by the ratio of the equivalent non-reference SAF to the equivalent reference SAF, which is equal to (1.09 / 5.22) or 0.2088.

Monoenergetic SAFs from the UFHADM and UFHADF hybrid reference phantoms were scaled with the UF photon cross-dose scaling technique to attempt to predict actual S values observed in the patient-specific phantoms. Uniformly distributed ^{131}I photons were simulated in the liver of each of the phantoms, and SAFs were calculated to a pancreas target in each phantom. Results from this validation study are given in Table 7. The percentage point gain in accuracy is relative to the UF scaling method. Scaling cross-dose photon SAFs for actual clinical application showed improvement for most of the patient-specific phantoms. A limiting factor for photon cross-dose scaling is the fact that most non-reference organs will not have the same shape as the reference models. Despite this limitation, gains in accuracy up to 9% were achieved using the proposed cross-dose scaling method.

Table 6. Excerpt of the photon cross-dose sphere SAFs (kg^{-1}) showing a subset of the source masses, target masses, photon energies, and center-to-center separations.

Source mass	Target mass	15.6 cm separation					31.3 cm separation				
		Photon energy (MeV)					Photon energy (MeV)				
(g)	(g)	1.000	1.500	2.000	3.000	4.000	1.000	1.500	2.000	3.000	4.000
1	1	7.51E-03	7.13E-03	6.51E-03	5.30E-03	5.29E-03	1.19E-03	1.20E-03	9.97E-04	1.09E-03	1.01E-03
	2	7.44E-03	6.78E-03	6.17E-03	5.39E-03	**5.22E-03**	1.19E-03	1.29E-03	1.07E-03	1.14E-03	1.04E-03
	4	7.46E-03	6.61E-03	6.20E-03	5.48E-03	5.14E-03	1.10E-03	1.14E-03	1.07E-03	1.10E-03	1.05E-03
	6	7.32E-03	6.55E-03	6.25E-03	5.59E-03	5.15E-03	1.09E-03	1.10E-03	1.10E-03	1.04E-03	1.05E-03
	8	7.27E-03	6.57E-03	6.27E-03	5.65E-03	5.11E-03	1.09E-03	1.11E-03	1.10E-03	1.03E-03	1.04E-03
	10	7.36E-03	6.66E-03	6.32E-03	5.69E-03	5.10E-03	1.11E-03	1.12E-03	1.12E-03	1.05E-03	1.02E-03
2	1	7.44E-03	6.78E-03	6.17E-03	5.39E-03	5.22E-03	1.19E-03	1.29E-03	1.07E-03	1.14E-03	1.04E-03
	2	7.36E-03	6.69E-03	6.17E-03	5.74E-03	5.38E-03	1.16E-03	1.17E-03	1.05E-03	1.01E-03	1.04E-03
	4	7.28E-03	6.50E-03	6.15E-03	5.76E-03	5.19E-03	1.12E-03	1.14E-03	1.10E-03	1.10E-03	**1.09E-03**
	6	7.20E-03	6.43E-03	6.24E-03	5.79E-03	5.18E-03	1.12E-03	1.11E-03	1.13E-03	1.08E-03	1.08E-03
	8	7.22E-03	6.49E-03	6.30E-03	5.78E-03	5.22E-03	1.10E-03	1.09E-03	1.10E-03	1.09E-03	1.04E-03
	10	7.26E-03	6.59E-03	6.30E-03	5.74E-03	5.22E-03	1.10E-03	1.10E-03	1.09E-03	1.10E-03	1.03E-03
4	1	7.46E-03	6.61E-03	6.20E-03	5.48E-03	5.14E-03	1.10E-03	1.14E-03	1.07E-03	1.10E-03	1.05E-03
	2	7.28E-03	6.50E-03	6.15E-03	5.76E-03	5.19E-03	1.12E-03	1.14E-03	1.10E-03	1.10E-03	1.09E-03
	4	7.29E-03	6.69E-03	6.22E-03	5.61E-03	5.11E-03	1.14E-03	1.15E-03	1.15E-03	1.03E-03	1.02E-03
	6	7.31E-03	6.69E-03	6.30E-03	5.78E-03	5.16E-03	1.13E-03	1.14E-03	1.13E-03	1.01E-03	1.03E-03
	8	7.27E-03	6.69E-03	6.39E-03	5.79E-03	5.15E-03	1.11E-03	1.11E-03	1.13E-03	1.02E-03	1.03E-03
	10	7.34E-03	6.74E-03	6.44E-03	5.80E-03	5.18E-03	1.14E-03	1.10E-03	1.11E-03	1.01E-03	1.03E-03

Table 7. Photon cross-dose scaling validation study showing predictive quality of UF scaling method as applied to patient-specific phantoms for ^{131}I photon dose to the pancreas from a source in the liver. The patient-specific naming convention is [gender][height in centimeters][weight in kilograms]
(e.g., m-193-132 is a 193 *cm* tall, 132 *kg* male).

Phantom	Actual Cross S value (mGy/MBq-s)	Reference Cross S value (mGy/MBq-s)	Predicted Cross S value (mGy/MBq-s)	Reference difference (%)	Predicted difference (%)	Percentage point gain (%)
Male						
m-193-132	8.95E-07	6.91E-07	7.18E-07	23	20	3
m-183-120	8.46E-07	6.91E-07	7.27E-07	18	14	4
m-183-112	8.92E-07	6.91E-07	7.19E-07	23	19	3
m-183-86	9.23E-07	6.91E-07	7.31E-07	25	21	4
m-180-82	1.37E-06	6.91E-07	8.14E-07	49	40	9
m-178-100	9.67E-07	6.91E-07	7.15E-07	28	26	2
m-178-73	7.01E-07	6.91E-07	6.81E-07	1	3	-2
m-175-81	1.19E-06	6.91E-07	7.44E-07	42	38	4
m-175-66	1.22E-06	6.91E-07	7.55E-07	43	38	5
m-173-98	7.39E-07	6.91E-07	6.50E-07	6	12	-6
m-173-74	1.12E-06	6.91E-07	7.54E-07	38	33	5
m-168-78	1.37E-06	6.91E-07	7.42E-07	50	46	4
m-165-74	1.83E-06	6.91E-07	8.26E-07	62	55	7
m-157-44	3.82E-06	6.91E-07	9.66E-07	82	75	7
Female						
f-164-59	1.20E-06	1.12E-06	1.09E-06	7	10	-3
f-175-136	1.48E-06	1.12E-06	1.20E-06	24	19	5
f-173-82	1.39E-06	1.12E-06	1.14E-06	19	18	1
f-165-63	1.37E-06	1.12E-06	1.11E-06	18	19	-1
f-163-117	8.43E-07	1.12E-06	1.06E-06	33	25	8
f-163-80	1.28E-06	1.12E-06	1.15E-06	12	10	2
f-160-61	1.60E-06	1.12E-06	1.13E-06	30	29	1
f-160-52	1.99E-06	1.12E-06	1.14E-06	44	43	1
f-160-51	2.39E-06	1.12E-06	1.22E-06	53	49	4
f-155-98	1.96E-06	1.12E-06	1.17E-06	43	40	3
f-155-70	1.62E-06	1.12E-06	1.16E-06	31	29	2
f-155-48	1.90E-06	1.12E-06	1.21E-06	41	36	5
f-152-66	1.07E-06	1.12E-06	1.15E-06	5	7	-2

4.4 Electron Cross-Dose

Surface shape and surface-to-surface distance heavily impact the magnitude of electron cross-dose SAF variation with changes in source and target size. A target tissue may be out of the range of primary electrons in the reference model, but within range of primary electrons in the non-reference model. When this is the case, electron dose differences between the two models may be orders of magnitude. Segmenting all internal organs in a patient CT image set in the clinic is impractical, so defining surface shape on a case-by-case basis was abandoned as a possible concept to assist in electron cross-dose scaling. Instead, the radiative component of the electron dose was selected as the scalable portion of electron dose.

The radiative component of electron dose can be attributed entirely to photons generated during the course of electron energy loss. Photon cross-dose scaling techniques could be applied in this case since the radiative component of electron simulations is effectively accomplished by photon transport. Collisional contributions to dose (primary dose) were not scaled and were subject to the uncertainties associated with changes in source-target shape and surface-to-surface distance. Principal gains in dosimetric accuracy were confined to the radiative component and therefore more distant organ pairs.

The patient-specific phantoms used for photon cross-dose scaling were also used for electron cross-dose validation. A uniform ^{90}Y beta source in the liver was simulated, and dose was recorded in the pancreas. Results from this study are given in Table 8. The organ dosimetry of most phantoms displayed a benefit when applying the UF electron cross-dose scaling method. Gains in accuracy were observed in most cases with a maximum gain of about 9% and average gain of about 2%. While this is not a drastic gain in accuracy, the majority of cases indicated that photon cross-dose scaling can be applied to the radiative component of electron cross-dose.

Table 8. Electron cross-dose scaling validation study showing predictive quality of UF scaling method as applied to patient-specific phantoms for ^{90}Y beta particle dose to the pancreas from a source in the liver. The patient-specific naming convention is [gender][height in centimeters][weight in kilograms]
(e.g., m-193-132 is a 193 cm tall, 132 kg male).

Phantom	Actual Cross S value (mGy/MBq-s)	Reference Cross S value (mGy/MBq-s)	Predicted Cross S value (mGy/MBq-s)	Reference difference (%)	Predicted difference (%)	Percentage point gain (%)
Male						
m-193-132	1.07E-08	7.30E-09	7.58E-09	32	29	3
m-183-120	9.30E-09	7.30E-09	7.66E-09	22	18	4
m-183-112	9.79E-09	7.30E-09	7.58E-09	25	23	2
m-183-86	1.05E-08	7.30E-09	7.71E-09	31	27	4
m-180-82	1.53E-08	7.30E-09	8.55E-09	52	44	8
m-178-100	1.03E-08	7.30E-09	7.54E-09	29	27	2
m-178-73	6.91E-09	7.30E-09	7.20E-09	6	4	2
m-175-81	1.69E-07	7.30E-09	7.83E-09	96	95	1
m-175-66	1.48E-08	7.30E-09	7.95E-09	51	46	5
m-173-98	7.17E-09	7.30E-09	6.88E-09	2	4	-2
m-173-74	1.41E-08	7.30E-09	7.94E-09	48	44	4
m-168-78	5.02E-08	7.30E-09	7.82E-09	85	84	1
m-165-74	2.13E-07	7.30E-09	8.68E-09	97	96	1
m-157-44	4.92E-08	7.30E-09	1.01E-08	85	79	6
Female						
f-164-59	1.38E-08	1.23E-08	1.18E-08	11	15	-3
f-175-136	3.05E-08	1.23E-08	1.30E-08	60	57	3
f-173-82	1.57E-08	1.23E-08	1.23E-08	22	21	1
f-165-63	1.67E-08	1.23E-08	1.20E-08	26	28	-2
f-163-117	9.00E-09	1.23E-08	1.14E-08	36	27	9
f-163-80	1.38E-08	1.23E-08	1.24E-08	11	10	1
f-160-61	4.97E-08	1.23E-08	1.22E-08	75	75	0
f-160-52	4.28E-07	1.23E-08	1.23E-08	97	97	0
f-160-51	5.55E-08	1.23E-08	1.31E-08	78	76	2
f-155-98	3.94E-08	1.23E-08	1.27E-08	69	68	1
f-155-70	2.60E-08	1.23E-08	1.25E-08	53	52	1
f-155-48	2.20E-08	1.23E-08	1.31E-08	44	40	4
f-152-66	1.06E-08	1.23E-08	1.24E-08	16	17	-1

5. Conclusions

This study found that updated self-dose scaling factors were of greater consequence than the cross-dose scaling factors, as the latter is not as sensitive to changes in source and target size as is the case for self-dose. These scaling factors allow a user of an internal dosimetry software to enter, when available, the masses of source/target organs, and in the case of cross-dose, the organ-to-organ centroid separation distance, whereby reference phantom SAFs for self-dose and cross-dose will be adjusted accordingly, and the S values then re-computed. Validation studies were performed and showed that in certain applications, the scaling factors improve patient organ dose estimates. For some cases, however, minimal to no increase in dose estimate accuracy was observed over the methods outlined originally in MIRD Pamphlet No. 11. Many dosimetry codes based upon the MIRD 11 methods assume a self-dose mass ratio scaling power of -0.667 for photons and -1.0 for electrons when in reality, self-dose scaling powers were found to vary between -0.357 and -0.996 for photons and between -0.600 and -1.000 for electrons over the energy ranges considered in this study. Applications where the UF scaling powers give better non-reference dose estimates were demonstrated and showed that personalized dosimetry could be improved through use of the UF scaling factors. Current internal dosimetry software does not scale reference phantom values of cross-dose, and thus many non-reference irradiation conditions are better predicted using the methods suggested here for patient-specific cross-dose scaling. Overall, the self- and cross-dose scaling methods proposed in this study may be effectively used to give more personalized patient dosimetry without patient-specific radiation transport simulations.

Acknowledgements

This research was supported in part by grants R01 CA116743 and R01 CA96441 with the National Cancer Institute, and by grant DE-FG07-06ID14773 with the US Department of Energy.

REFERENCES

Bolch W, Lee C, Wayson M and Johnson P 2010 Hybrid computational phantoms for medical dose reconstruction *Radiat Environ Biophys* **49** 155-168

Bolch W E, Eckerman K F, Sgouros G and Thomas S R 2009 MIRD Pamphlet No. 21: A generalized schema for radiopharmaceutical dosimetry: Standardization of nomenclature *J Nucl Med* **50** 477-484

Clark L D, Stabin M G, Fernald M J and Brill A B 2010 Changes in radiation dose with variations in human anatomy: moderately and severely obese adults *J Nucl Med* **51** 929-932

Cristy M and Eckerman K F 1987 *Specific absorbed fractions of energy at various ages from internal photon sources* (Oak Ridge National Laboratory)

ICRP 1980 *ICRP Publication 30: Limits for intakes of radionuclides by workers* (International Commission on Radiological Protection)

ICRP 2002 ICRP Publication 89: Basic anatomical and physiological data for use in radiological protection - reference values *Ann ICRP* **32** 1-277

ICRP 2008 ICRP Publication 107: Nuclear decay data for dosimetric calculations *Ann ICRP* **38** 1-26

ICRP 2015 ICRP Publication 130 - Occupational Intakes of Radionuclides: Part 1 *Ann ICRP* **44** 1-188

ICRU 1992 *ICRU Report 46: Photon, electron, proton and neutron interaction data for body tissues* (International Commission on Radiation Units and Measurements)

Johnson P B, Geyer A, Borrego D, Ficarrotta K, Johnson K and Bolch W E 2011 The impact of anthropometric patient-phantom matching on organ dose: a hybrid phantom study for fluoroscopy guided interventions *Med Phys* **38** 1008-1017

Kim H S, Yeom Y S, Nguyen T T, Choi C, Han M C, Lee J K, Kim C H, Zankl M, Petoussi-Henss N, Bolch W E, Lee C, Qiu R, Eckerman K and Chung B S 2017 Inclusion of thin target and source regions in alimentary and respiratory tract systems of mesh-type ICRP adult reference phantoms *Phys Med Biol* **62** 2132-2152

Lee C, Lodwick D, Hurtado J, Pafundi D, Williams J L and Bolch W E 2010 The UF family of reference hybrid phantoms for computational radiation dosimetry *Phys Med Biol* **55** 339-363

Marine P M, Stabin M G, Fernald M J and Brill A B 2010 Changes in radiation dose with variations in human anatomy: larger and smaller normal-stature adults *J Nucl Med* **51** 806-811

Petoussi-Henss N, Bolch W E, Zankl M, Sgouros G and Wessels B 2007 Patient-specific scaling of reference S-values for cross-organ radionuclide S-values: what is appropriate? *Radiat Prot Dosimetry* **127** 192-196

Snyder W S, Ford M R, Warner G G and Watson S B 1975 *MIRD Pamphlet No. 11: S, absorbed dose per unit cumulated activity for selected radionuclides and organs* (Society of Nuclear Medicine)

Stabin M G and Konijnenberg M W 2000 Re-evaluation of absorbed fractions for photons and electrons in spheres of various sizes *J Nucl Med* **41** 149-160.

Stabin M G, Xu X G, Emmons M A, Segars W P, Shi C and Fernald M J 2012 RADAR Reference Adult, Pediatric, and Pregnant Female Phantom Series for Internal and External Dosimetry *J Nucl Med* **53** 1807-1813

Wayson M B 2012 *Computational internal dosimetry methods as applied to the University of Florida series of hybrid phantoms.* Biomedical Engineering, University of Florida, Dissertation.

Wayson M B and Bolch W E in review Individualized adjustments to reference phantom internal organ dosimetry - Scaling factors give knowledge of patient external anatomy *Phys Med Biol*

Xu X G and Eckerman K F 2009 *Handbook of anatomical models for radiation dosimetry* (London, UK: Taylor & Francis)

Xu X G, Taranenko V, Zhang J and Shi C 2007 A boundary-representation method for designing whole-body radiation dosimetry models: pregnant females at the ends of three gestational periods--RPI-P3, -P6 and -P9 *Phys Med Biol* **52** 7023-7044

Yeom Y S, Kim H S, Nguyen T T, Choi C, Han M C, Kim C H, Lee J K, Zankl M, Petoussi-Henss N, Bolch W E, Lee C and Chung B S 2016a New small-intestine modeling method for surface-based computational human phantoms *Journal of radiological protection : official journal of the Society for Radiological Protection* **36** 230-245

Yeom Y S, Wang Z J, Nguyen T T, Kim H S, Choi C, Han M C, Kim C H, Lee J K, Chung B S, Zankl M, Petoussi-Henss N, Bolch W E and Lee C 2016b Development of skeletal system for mesh-type ICRP reference adult phantoms *Phys Med Biol* **61** 7054-7073

Zhang J, Na Y H, Caracappa P F and Xu X G 2009 RPI-AM and RPI-AF, a pair of mesh-based, size-adjustable adult male and female computational phantoms using ICRP-89 parameters and their calculations for organ doses from monoenergetic photon beams *Phys Med Biol* **54** 5885-5908